Semiclassical ground-state phase diagram and multi-Q phase of a spin-orbit coupled model on triangular lattice

Changle Liu,[1] Xiaoqun Wang,[2,1] and Rong Yu[1,2]

[1] *Department of Physics, Renmin University of China, Beijing 100872, China*
[2] *Department of Physics and Astronomy, Shanghai Jiao Tong University, Shanghai 200240, China and Collaborative Innovation Center for Advanced Microstructures, Nanjing 210093, China*

arXiv:1607.02295v1 [cond-mat.str-el] 8 Jul 2016

Motivated by recent experiments on the frustrated quantum magnetic compound $YbMgGaO_4$, we study an effective spin model on triangular lattice taking into account the effects of the spin-orbit coupling. We determine the classical ground-state phase diagram of this model, which includes a 120° Néel and two collinear antiferromagnetic phases. In the vicinity of the phase boundary between the Néel and collinear phases, we identify three intermediate non-collinear antiferromagnetic phases. In each of them the magnetic moments are ordered at multiple incommensurate wave vector **Q** values. We further study the effects of quantum fluctuations in this model via a linear spin-wave theory. We find that the spin excitation gap of the non-collinear multi-**Q** antiferromagnetic state is finite but can be vanishingly small, and this state is unstable to a spin liquid phase under strong quantum fluctuations in some large $|J_{z\pm}|$ regime.

I. INTRODUCTION

Frustrated magnets can hold exotic states of matter, such as a quantum spin liquid (QSL) in which the spin rotational and time reversal symmetries are preserved down to the temperature of absolute zero.[1] In the search of QSL, the triangular antiferromagnet is one of the most well studied frustrated systems. By disturbing the 120° long-range antiferromagnetic order of the Heisenberg model with certain tuning parameters, various QSL states on triangular lattice have been proposed.[2–6] Alternatively, strong spin-orbit coupling (SOC) may introduce non-Heisenberg exchange couplings and is found to be an effective way in stabilizing some exotic quantum states, including a QSL, of frustrated magnets.[7–10] Recently, a new triangular antiferromagnet with strong SOC, $YbMgGaO_4$, has been proposed to be a candidate compound of gapless QSL.[11,12] In this material, it is shown that the strong SOC gives rise to large spin and spatial entangled anisotropic interactions, which are suggested to be crucial in stabilizing a QSL ground state.[11,12]

An effective model Hamiltonian for $YbMgGaO_4$ has been proposed in Ref.[11]. It contains strong anisotropic non-Heisenberg interactions due to SOC. But little is known for this model. Even the classical phase diagram of this model has not been well studied. And it is still unclear whether these anisotropic non-Heisenberg terms in the model would provide sufficiently strong quantum fluctuations to stabilize a QSL, and how would such a state be relevant to the likely QSL phase observed in experiments. To address these questions, we investigate the ground-state phase diagram and spin excitations of this model. We determine the classical ground-state phase diagram by numerical optimization and a modified Luttinger-Tisza (LT) method. The phase diagram contains a 120° Néel antiferromagnetic (AFM) phase, two collinear AFM phases, and three novel incommensurate non-collinear AFM phases. In these incommensurate phases, the magnetic moments are ordered at multiple **Q** wave vectors. By using the linear spin-wave theory, we find that all these classical magnetic phases survive in the presence of weak quantum fluctuations. We further calculate the spin-wave excitation in the non-collinear multi-**Q** phase and find the spin excitation gap of this state is finite but can be vanishingly small. When the quantum fluctuations are strong, we find that a spin liquid phase can be stabilized in the phase diagram.

The paper is organized as follows: In Sec. II, we present the general effective spin model and outline the methods we used to study its ground state and spin excitations. In Sec. III, we determine the classical ground-state phase diagram of this model by using a numerical zero-temperature energy optimization with the aid of a modified LT method, and show that non-collinear multi-**Q** phases are stabilized in certain regimes of the phase diagram. In Sec. IV, we show the spin excitations within the linear spin-wave calculations and the correction of the quantum fluctuations to the ground-state phase diagram. We further discuss the implication of the model and our results to the $YbMgGaO_4$ in Sec. V. Finally we draw conclusions in Sec. VI.

II. MODEL AND METHODS

In $YbMgGaO_4$, because of the strong spin-orbit coupling (SOC), the electrons of the Yb^{3+} ion are in a state of total angular momentum $J = 7/2$. The crystal field then splits it into a series of Kramers doublets. At low temperatures, only the lowest Kramers doublet is relevant and the system can be described by a model of interacting effective spin-1/2 magnetic moments. Due to the separation between the two Yb layers by the nonmagnetic Mg/GaO_5 layers, the interlayer superexchange coupling between the effective moments are very weak. We then neglect this interlayer exchange coupling, and define the model on a two-dimensional triangular lattice.

The Hamiltonian of this model reads[11]

$$\begin{aligned} H = \sum_{\langle ij \rangle} [& J_{zz} S_i^z S_j^z + J_{\pm} (S_i^+ S_j^- + S_i^- S_j^+) \\ & + J_{\pm\pm} (\gamma_{ij} S_i^+ S_j^+ + \gamma_{ij}^* S_i^- S_j^-) \\ & - \frac{i J_{z\pm}}{2} (\gamma_{ij}^* S_i^+ S_j^z - \gamma_{ij} S_i^- S_j^z + \langle i \leftrightarrow j \rangle)] \end{aligned} \tag{1}$$

Here $\mathbf{S}_i$ refers to the effective spin-1/2 magnetic moment, and J_{zz}, $J_{\pm}$, $J_{\pm\pm}$, and $J_{z\pm}$ are exchange couplings between nearest neighbor moments. In this paper, we are interested in the case $J_{zz} > 0$, which is relevant to the $YbGaMgO_4$ compound[11]. The coefficients γ_{ij} are defined on each bond of the triangular lattice which take the value 1, $e^{i\frac{2\pi}{3}}$ and $e^{-i\frac{2\pi}{3}}$ for $\pm\mathbf{a}_1$, $\pm\mathbf{a}_2$ and $\pm\mathbf{a}_3$ nearest-neighor bond directions, respectively. See Fig. 1(a). The SOC couples the rotational symmetry in the spin space to that in the real-space. This lowers the symmetry of the model from SU(2) to D_{3d}. Therefore, the model is non-Heisenberg, with spin and spatial anisotropic exchange couplings described by J's and γ_{ij}. Due to the effect of SOC, this Hamiltonian has only *discrete* time-reversal and D_{3d} point group symmetries, but the ground state may still contain some emergent continuous symmetry, as will be discussed in detail below.

A powerful way to investigate the classical ground-state configuration of spin models is the Luttinger-Tisza method[13]. In this approach, one first performs the Fourier transformation for $\mathbf{S}_j$,

$$\mathbf{S}_j = \sqrt{\frac{1}{N}} \sum_{\mathbf{k}} \mathbf{S}_{\mathbf{k}} e^{i\mathbf{k}\cdot\mathbf{R}_j}, \tag{2}$$

where the sum is taken in the first Brillouin zone. The Hamiltonian in Eq. (1) can then be rewritten to a tensor form

$$H = \sum_{\mathbf{k}} \mathbf{S}_{\mathbf{k}}^* \cdot \mathsf{J}_{\mathbf{k}} \cdot \mathbf{S}_{\mathbf{k}}, \tag{3}$$

where $\mathsf{J}_{\mathbf{k}}$ is a real symmetric tensor, taking into account the symmetry of the model, and $\mathbf{S}_{\mathbf{k}}^*$ refers to the complex conjugate of $\mathbf{S}_{\mathbf{k}}$. It is then diagonalized to be

$$H = \sum_{\mathbf{k}\mu} \omega_{\mathbf{k}\mu} S_{\mathbf{k}\mu}^* S_{\mathbf{k}\mu}, \tag{4}$$

where $S_{\mathbf{k}\mu} = \mathbf{S}_{\mathbf{k}} \cdot \hat{\mathbf{e}}_{\mathbf{k}\mu}$, $\omega_{\mathbf{k}\mu}$ and $\hat{\mathbf{e}}_{\mathbf{k}\mu}$ are corresponding eigenvalues and orthorgonal eigenvectors of the tensor $\mathsf{J}_{\mathbf{k}}$. Meanwhile, the local constraint of the constant spin magnitude at an arbitrary site j,

$$\mathbf{S}_j \cdot \mathbf{S}_j = S^2, \tag{5}$$

yields the equivalent hard constraints on $\mathbf{S}_{\mathbf{k}}$ for any wave vector $\mathbf{q}$:

$$\frac{1}{N} \sum_{\mathbf{k}} \mathbf{S}_{\mathbf{k}} \cdot \mathbf{S}_{\mathbf{q}-\mathbf{k}} = S^2 \delta_{\mathbf{q}\mathbf{G}}, \tag{6}$$

where $\mathbf{G}$ is a reciprocal lattice vector. Also, since $\mathbf{S}_j$ are real vectors, each Fourier component must satisfy the relation

$$\mathbf{S}_{\mathbf{k}}^* = \mathbf{S}_{-\mathbf{k}} \tag{7}$$

In the original LT method, one minimizes the energy in Eq. (4) under a released global constraint

$$\frac{1}{N} \sum_{\mathbf{k}} |\mathbf{S}_{\mathbf{k}}|^2 = S^2, \tag{8}$$

i.e., by taking $\mathbf{q} = \mathbf{G}$ in Eq. (6). If the corresponding spin configuration of the minimum turns out to satisfy Eq.(7) and all local constraints in Eq.(6) as well, it must be the true physical ground state.

This method works well for conventional Heisenberg or XXZ models in some parameter regimes. However, it has been showed that the LT method failed to produce the physical ground state of the Hamiltonian in Eq. (1) because those hard constraints in Eq. (6) cannot be all satisfied simultaneously[14]. The deep underlying reason is that the tensor $\mathsf{J}_{\mathbf{k}}$ of the Hamiltonian contains only very low discrete symmetries, which will be discussed in Appendix A.

To obtain the classical ground state of this model, we perform numerical zero-temperature energy minimization of spin configurations in large clusters. We find that besides the ordinary 120° Néel and collinear phases discovered in the previous work, in the vicinity of the Néel-collinear phase boundary, there exists three new phases in which spins are ordered at multiple incommensurate $\mathbf{Q}$ points. We denote these phases as "multi-$\mathbf{Q}$" phases. These multi-$\mathbf{Q}$ phase properties and the subtle phase transition to collinear phase can be well produced in a modified LT approach, by taking into account all the constraints in Eq. (6). More details of this method is given in Appendix A.

To study the spin excitations and the effects of quantum fluctuations to the classical ground states, we apply a linear spin-wave theory[15–17] in real space by performing a local rotation on each spin $\mathbf{S}_i$. The dynamical structure factor are calculated using the spinW codecs[15]. Details of the spin-wave approach is given in Appendix B.

III. CLASSICAL GROUND-STATE PHASE DIAGRAM AND THE MULTI-Q STATE

A. The phase diagram

The model in Eq. (1) has a rich phase diagram even for classical spins. Let us first take a look at a special case where $J_{zz} = 2J_{\pm} - 2J_{\pm\pm} \equiv J_H$ and $J_{z\pm} = 0$. In this case, Eq. (1) reduces to a Heisenberg-120°-compass model[8]

$$H = \sum_{\langle ij \rangle} (J_H \mathbf{S}_i \cdot \mathbf{S}_j + J_c S_i^a S_j^a), \tag{9}$$

where $J_c = 4J_{\pm\pm}$ and a refers to the direction of the bond $\langle ij \rangle$. To simplify the discussion, let us define $\alpha = J_c/(J_H + J_c)$.

It is known that in the Heisenberg limit ($\alpha = 0$), the ground state of this model is the 120° Néel AFM state[18,19], in which all spins lie in the plane of the lattice. While in the compass limit ($\alpha = 1$), the ground state is a collinear AFM state[20], in which all spins order ferromagnetically along one bond direction but antiferromagnetically along the other two. See Fig. 1(b)(c).

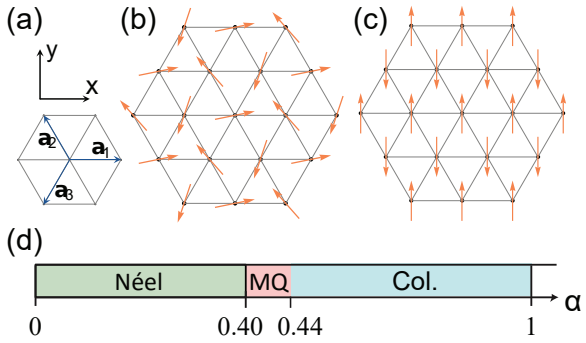

FIG. 1. (a): Definition of the coordinate system and the nearest-neighbor bonds. (b),(c): Spin patterns of the Néel and the collinear phases. (d): The classical ground-state phase diagram of the Heisenberg-120°-compass model. Here the collinear and the multi-**Q** phases correspond to the collinear II and multi-**Q** II phases in the generic phase diagram of Fig. 2(a) at $J_{z\pm} = 0$, respectively.

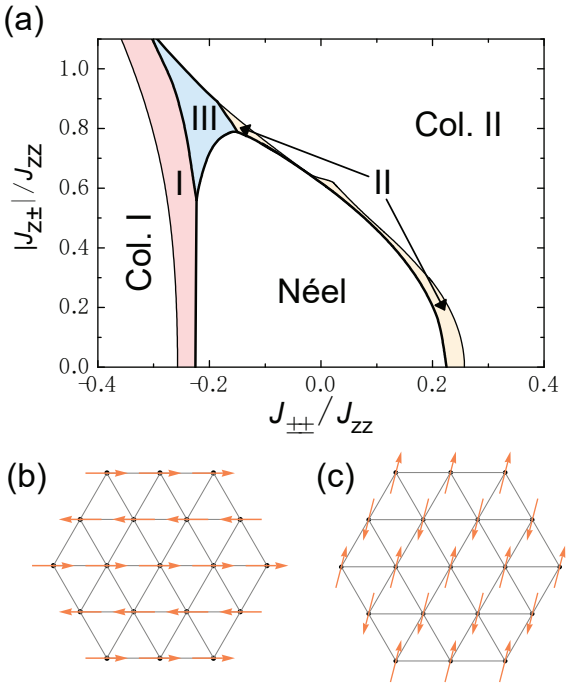

FIG. 2. (a): Classical ground-state phase diagram of the generic spin-orbit model defined in Eq. (1). Thicker and thinner curves refer to first- and second-order transitions, respectively. Colored regimes labeled as I, II, III correspond to the three multi-**Q** phases discussed in the text. Sketch of real-space spin patterns of the the two collinear states. The Néel phase is as same as the one shown in Fig. 1(b).

Knowing the phases in the two limiting cases, we optimize the total energy in large clusters to explore the ground state of a general coupling α. We find that the Néel state remains to be the classical ground state for $\alpha < 0.40$. Although the Hamiltonian has only discrete symmetry when the system is away from the Heisenberg point at $\alpha = 0$, in the Néel state the spin configurations still have degenerate energies under a global rotation in the spin space with an arbitrary angle ϕ about the z axis. This is an example of an emergent $U(1)$ symmetry of the ground state. As α further increases, we find an incommensurate noncollinear AFM for $0.40 < \alpha < 0.44$, as shown in Fig. 1(d). This state is denoted as the multi-**Q** state as the magnetic moments are ordered at multiple wave vectors in this state. Here we describe the phase diagram, and defer the discussion on the nature of the multi-**Q** state to Sec. III B. At $\alpha \approx 0.40$, we find a first-order transition between the Néel AFM and the multi-**Q** state, while at $\alpha \approx 0.44$, the system undergoes a second-order transition from the multi-**Q** phase to the collinear AFM states.

Compared to the Heisenberg-120°-compass model, the full model in Eq. (1) contains additional anisotropic terms. In our paper, the ratio $J_\pm/J_{zz}$ is fixed to be 0.9, an input from the experimental results of the $YbGaMgO_4$ single crystals[11]. But the phase diagram is similar for other $J_\pm/J_{zz} > 0.5$ values. Our numerical energy optimization result reveals that the ground-state phase diagram still contains Néel, collinear, and multi-**Q** phases. The emergent $U(1)$ symmetry of the Néel phase also exists for this model. The multi-**Q** phase lies in between the collinear and the Néel AFM phases, as shown in Fig. 2(a). When $J_{z\pm} = 0$, the groundstates (so do the Hamiltonians) with opposite signs of $J_{\pm\pm}$ are connected by 90° rotation in spin space about the z axis.

For $J_{z\pm} \neq 0$, the two collinear phases with opposite $J_{\pm\pm}$ values are no longer equivalent. In the collinear I phase spins are still aligned along one bond direction while in the collinear II phase spins are aquired to have finite z components so as to further minimize the energy. Two multi-**Q** states at either side of the Néel phase (which we denote as multi-**Q** I and multi-**Q** II phases, respectively) are not equivalent either. Nor do they lie in the xy plane. But both of them coplanar. Also, we find that the multi-**Q** I to collinear I and multi-**Q** II to collinear II transitions are second-order, while all other transitions are first-order. Néel AFM state can be stabilized at a vast range of $J_{\pm\pm}$ and $J_{z\pm}$ values.

When $J_{z\pm}$ is large, phase(donated as multi-**Q** III phase) is stabilized on the upper side of the Néel regime, where the spins are non-coplanar, and have relatively large from the spin directions in the collinear II order. The phase transitions between the multi-**Q** III phase to

others are first-order.

B. Nature of the multi-Q phase

One can easily check that the collinear state satisfy local constraints in Eq. (6), and for sufficiently large $|J_{\pm\pm}|$, the minimum of the eigenvalue of the tensor $\mathsf{J}_{\mathbf{k}}$ is located at the wave vector $\mathbf{Q}_0 = (0, 2\pi/\sqrt{3})$, the ordering wave vector of the collinear state. According to the LT method, the collinear state must be the exact ground state of the model in this regime. However, when $|J_{\pm\pm}|$ is decreased towards the boundary between the collinear and the Néel states, the minimum of the eigenvalues of the tensor $\mathsf{J}_{\mathbf{k}}$ is away from the wave vector $\mathbf{Q}_0$, while the energy minimum produced by the LT method no longer satisfy all local constraints. Therefore, in this $|J_{\pm\pm}|$ regime, the LT method fails to give the correct ground state configuration of the system.

By taking the numerical energy minimization analysis, we find that as $|J_{\pm\pm}|$ decreases so that the minimum of the eigenvalues of $\mathsf{J}_{\mathbf{k}}$ deviates from $\mathbf{Q}_0$, the ground state of the system does not immediately change. The collinear state remains to be the ground state at this stage. However, as $|J_{\pm\pm}|$ further decreases, depending on the ratio of $|J_{z\pm}/J_{zz}|$, the system may enter the intermediate multi-$\mathbf{Q}$ state via either a first- or a second-order transition, as shown in Fig. 2(a). We find that these multi-$\mathbf{Q}$ phases can be well reconstructed by introducing *finite* Fourier components $\mathbf{S}_{\mathbf{Q}}$'s on multiple $\mathbf{Q}$'s based on the original collinear states so as to minimize the energy on the premise of satisfying local constraints (8). The detail of the process is given in the Appendix A.

Here we summarize the key results. We find that in multi-$\mathbf{Q}$ states the magnetic moments are ordered at multiple wave vectors, as shown in Fig. 3(a)(c). The spin structure factor shows a primary peak at wave vector $\mathbf{Q}_0$, the ordering wave vector of the collinear state. Two secondary peaks are present at incommensurate wave vectors $\pm\mathbf{Q}_1$ along some high symmetry line. For multi-$\mathbf{Q}$ I/II states, their spectral weights of $\pm\mathbf{Q}_1$ are in general about one order of magnitude smaller than the primary one. Other finite peaks of the structure factor, for example, the peaks $\mathbf{Q}_2 = [2\mathbf{Q}_1 - \mathbf{Q}_0]$, are also present, as shown in Fig. 3(a)(c). Here the symbol $[\mathbf{k}]$ represents the equivalent $\mathbf{k}$ point in the first Brillouin zone. In fact, we reveal that in order to satisfy all local constraints, in principle one need to introduce *finite* Fourier components for an *infinite* series of wave vectors $\mathbf{Q}_n$. But their spectral weights decays exponentially with increasing n. For example, here the spectral weight of the peak at $\mathbf{Q}_2$ is already about several orders of magnitudes smaller than that of the primary peak. In practice, for multi-$\mathbf{Q}$ I and II phases, the peaks at $\mathbf{Q}_n$ for $n > 2$ can hardly be detected and have no physical significance. Therefore, as a good approximation of the ground state, the series can be truncated at $n = 2$. For multi-$\mathbf{Q}$ III phase where the weight of $\mathbf{Q}_2$ and $\mathbf{Q}_1$ have been comparable to $\mathbf{Q}_0$, since the spectra weight of $\mathbf{Q}_n$ for $n > 2$ is still small, our perturbative construction are still qualitatively valid to produce the spin configurations.

Sketches of the real-space spin pattern of the multi-$\mathbf{Q}$ state are shown in Fig. 3(b)(d). Take multi-$\mathbf{Q}$ I state for example: In a simple case $J_{z\pm} = 0$, the spins all lie in the plane of the lattice. The spin pattern exhibits additional modulation on top of the collinear order, but does not form any spiral order. By taking the above truncation, the angle ϕ_i that a spin at site $\mathbf{R}_i$ deviates from the horizontal direction can be expressed as $\phi_i = \sin^{-1}[A\sin(\mathbf{Q}_1 \cdot \mathbf{R}_i + \phi_0)]$ and $\phi_i = \pi - \sin^{-1}[A\sin(\mathbf{Q}_1 \cdot \mathbf{R}_i + \phi_0)]$ for alternating rows respectively, where $A = \frac{2|\mathbf{S}_{\mathbf{Q}_1}|}{N\sqrt{S}}$, defined as the modulation amplitude, and ϕ_0 is an arbitrary angle related to the phase of the Fourier component $\mathbf{S}_{\mathbf{Q}_1}$. Here A scales the deviation to the collinear order. If we take A as a variational parameter and calculate the energy of the spin pattern defined by $\phi_i[A]$, we see (from Fig. 4) that the energy of the collinear state (corresponding to $A = 0$) is a local maximum while the energy of the multi-$\mathbf{Q}$ state (at $A \approx 0.35$) is the minimum. This verifies that the multi-$\mathbf{Q}$ state, instead of the collinear one, is the ground state of the model in the vicinity of the Néel-collinear phase boundary of the phase diagram.

For multi-$\mathbf{Q}$ I and II states, despite the relatively large deviation of multi-$\mathbf{Q}$ states from the collinear ones, we can see from Fig. 4 that their energy difference are generally neglectably small. While in large $|J_{z\pm}|$ regime, the non-coplanar spin patten of the multi-$\mathbf{Q}$ III state can much more energy than state. Also, we can see that around the multi-$\mathbf{Q}$ energy minimum, there exists large numbers of competing states with different modulation amplitude A, wavevector $\mathbf{q}$ and phase ϕ_0 close in similar energy scale. These competing states are in destablizing magnetic moments when thermal or quantum fluctuations are switched on.

IV. EFFECTS OF QUANTUM FLUCTUATIONS AND SPIN EXCITATIONS IN THE MULTI-Q PHASE

To investigate the spin excitations of the above antiferromagnetic phases, we perform a linear spin wave(LSW) analysis. The detail of the LSW method is given in the Appendix.

For the Néel, multi-$\mathbf{Q}$, and collinear states, the corresponding dynamical structural factor, defined as,

$$S^{\mu\nu}(\mathbf{k},\omega) = \frac{1}{2\pi N}\sum_{ij}\int_{-\infty}^{+\infty} \mathrm{d}t\, e^{i\mathbf{k}\cdot(\mathbf{r}_i-\mathbf{r}_j)-i\omega t}\langle S_i^{\mu} S_j^{\nu}(t)\rangle, \tag{10}$$

are shown in Fig. 5 for comparison. In the Néel state, the spin excitation is gapless at M point of the Brillouin zone, as a consequence of the emergent $U(1)$ symmetry mentioned in Sec. III. As for the collinear state, the spin excitations are gapped, reflecting the discrete

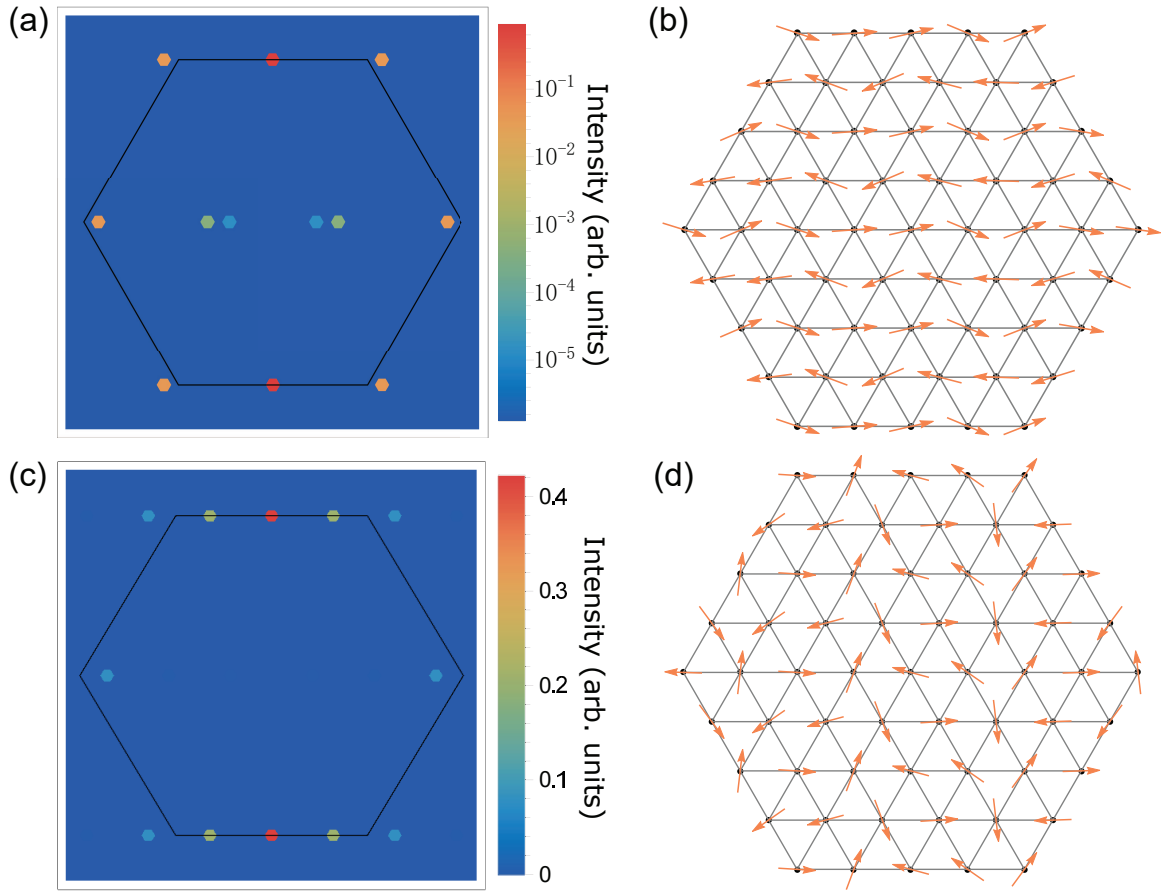

FIG. 3. Color maps of the static structure factor and the sketchs of the real-space spin pattern (projected to the xoy plane) of: the coplanar multi-**Q** I state (in (a),(b)) and the non-coplanar multi-**Q** III state (in (c),(d)). Here the model parameters we take for the multi-**Q** I state are $J_{\pm\pm} = -0.2165$, $J_{z\pm} = 0$, and for the multi-**Q** III state are $J_{\pm\pm} = -0.19$, $J_{z\pm} = 0.85$.

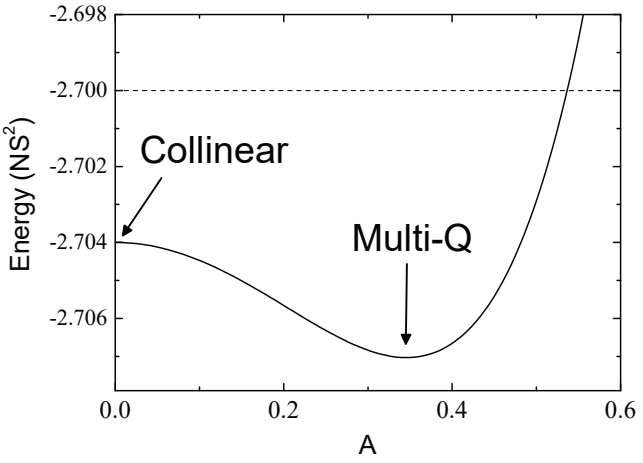

FIG. 4. Energy versus modulation amplitude A for the variational configuration $\{\phi_i[A]\}$. Here we take the $J_{\pm\pm} = -0.226$ and $J_{z\pm} = 0$. Dashed line shows the energy of the Néel state.

symmetry of the model. The minimum of the spin-wave dispersion is located at an incommensurate wave vector $\mathbf{Q}_1$ along some high symmetry line. For moderate $J_{z\pm}$, when approaching to the collinear-to-multi-$\mathbf{Q}$ phase boundary by decreasing $|J_{\pm\pm}|$, the spin gap at $\mathbf{Q}_1$ drops to zero. Further decreasing $|J_{\pm\pm}|$, the spin-wave dispersion of the collinear state near $\mathbf{Q}_1$ becomes imaginary, indicating that the incommensurate magnon is condensed and the multi-$\mathbf{Q}$ phase develops. This is consistent with the collinear-to-multi-$\mathbf{Q}$ transition in the classical phase diagram. We also claim that along the collinear-II-to-multi-$\mathbf{Q}$-II boundary in Fig. 2(a), collinear II phase is destablized at different $\mathbf{Q}_1$ points for different parameters, which makes the boundary zig-zag.

Spin-wave excitation spectra of the multi-$\mathbf{Q}$ I/II state look similar to those of the collinear phase in a large portion of the Brilluion zone. But due to its complicated real-space spin structure, the spectra of the multi-$\mathbf{Q}$ state contain multiple shadow branches, which are most significantly seen near the M point. For multi-$\mathbf{Q}$ III states, the spectra seems further scattered due to the large modulation of incommensurate components. Particularly in certain intermediate energy regime, sharp spin-wave dispersion may not be well observed due to the various shaddow bands of magnons that are associated with the complicated real-space spin pattern of the multi-$\mathbf{Q}$ phase. Surprisingly, we find the spin gap of multi-$\mathbf{Q}$ I/II and large portion of multi-$\mathbf{Q}$ III states is vanishingly small. This suggests existence of an (approximate) emergent $U(1)$ symmetry. While this is not as obvious as in the Néel phase, we can understand it in an intuitive way. Taking the Fourier component $\mathbf{S}_{\mathbf{Q}_1}$ as a variational parameter, near the energy minimum (corresponding to the multi-$\mathbf{Q}$ ground state), the energy depends weakly on the phase of $\mathbf{S}_{\mathbf{Q}_1}$. The excitations along the phase direction (transverse direction to the amplitude excitations) are then almost gapless, and develop an approximate Goldstone mode at $\mathbf{Q}_1$. Nevertheless in some multi-$\mathbf{Q}$ III regime (close to the Néel AFM phase), the spin excitation gap can be sizable.

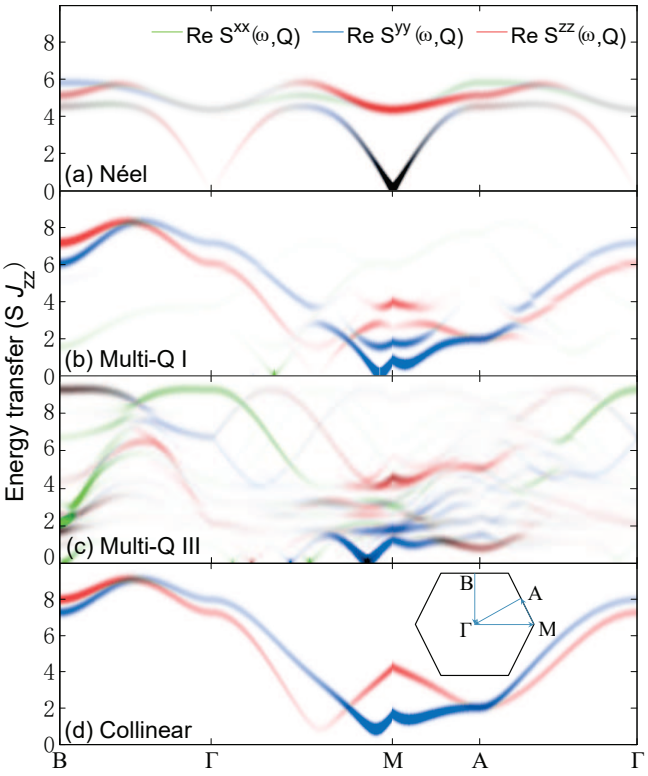

FIG. 5. Dynamical structure factors of Néel, multi-$\mathbf{Q}$, and collinear phases, respectively. The parameters for the Néel and multi-$\mathbf{Q}$ I phase are $J_{\pm\pm} = -0.2165$, $J_{z\pm} = 0$, for the multi-$\mathbf{Q}$ III phase are $J_{\pm\pm} = -0.19$, $J_{z\pm} = 0.85$, and for the collinear phase are $J_{\pm\pm} = -0.28$, $J_{z\pm} = 0$. The thickness of the color in each curve is proportional to the magnon spectral weight.

The LSW approach also allows us to exam the effects of quantum fluctuations to the classical phases. Here we show the $1/S$ vs $J_{\pm\pm}/J_{zz}$ phase diagram in LSW theory at zero temperature in Fig. 6. For $J_{z\pm} = 0$ case, Néel, collinear, and multi-$\mathbf{Q}$ states all survive weak to moderate quantum fluctuations. But the ordered magnetic moments are reduced by quantum fluctuations. For Néel and collinear states, the moment reduction is uniform for each sublattice, while in multi-$\mathbf{Q}$ states, due to the complicated magnetic structure, the moment reduction is inhomogeneous, and depends on the neighboring environment of a spin in each sublattice. In each phase the (largest) ordered moment reduction at is found to be $\lesssim 0.16$, so that the magnetic orders are robust even for $S = 1/2$. In our calculation a spin liquid phase can be stabilized for $1/S \gtrsim 7$ where quantum fluctuations are sufficiently strong.

When $|J_{z\pm}|$ is large, the phase diagram changes quite a bit, as shown in Fig 6(b). We find that all phases become further unstable against quantum fluctuations. Particularly, the ordered moment reduction of the Néel

state can be as large as 0.3, and it can only be stabilized as a metastable state since taking into account the quantum corrections, its energy is higher than that of other ordered states. moment reduction can be as large as around 0.3. The multi-**Q** phase is completely unstable to a spin liquid at $1/S \approx 3$. In this sense, the system in this parameter regime is very close to a spin liquid phase for $S = 1/2$.

V. DISCUSSIONS

Magnetic order at multiple **Q** vectors usually exists in systems with a complex lattice structure or competing exchange interactions such that the magnetic unit cell contains more than one magnetic ion.[21] The multi-**Q** phase we studied in this paper exists in simple triangular lattice with nearest-neighbor exchange couplings. It is induced by the anisotropic $J_{\pm\pm}$ interaction of the model, which introduces strong competition between the 120° Néel and the collinear phases. At low temperatures, the system attempts to order at both wave vectors $\mathbf{Q}_0$ and $\mathbf{Q}_{\rm N}$, and the multi-**Q** state is eventually stabilized as a compromise. In fact, the existence of a large number of energetically competing configurations around the multi-**Q** ground state is evidenced by the shallow energy profile around the minimum in Fig. 3. The competition around the multi-**Q** ground state gives rise to enhanced thermal fluctuations which can suppress the ordering temperature of the multi-**Q** state. Actually, the reduction of ordering temperature near the boundary between the Néel and collinear phases has been observed in a recent Monte Carlo study[12]. But the multi-**Q** was not resolved in the Monte Carlo calculation due to the limited system size and energy resolution.

Our LSW result shows that in some large $J_{z\pm}$ regime the system can be close to QSL state for $S = 1/2$ in this model. It should be noted that in cases where S is small and quantum fluctuation is large, magnon interactions may significantly renormalize the system and LSW approximation may become no longer valid. Therefore, it is possible that magnon interactions may further supress the magnetic order and drive the system towards a spin liquid. Also, as a semiclassical approximation, spin wave theory considers quantum fluctuations above only *one* classically ordered state. In fact, quantum fluctuations also allow tunnelling among different classical configurations with similar energies. For multi-**Q** states, there exists large numbers of competing states with similar energies (Néel, and other multi-**Q** configurations with different **K** and $\mathbf{S}_{\mathbf{K}}$). Quantum(and thermal) tunneling among these states may significantly destabilize the magnetic order. On the other hand, the classical configuration of multi-**Q** state in real space looks much more "disordered" than other conventional magnetic phases, such as the Néel and collinear AFM states. Such a disordered nature also shows up at the linear spin-wave level: the ordered moment reduction is inhomogeneous. This makes the multi-**Q** state susceptible to quantum fluctuations: once the quantum fluctuation $1/S$ increases to the value such that the ordered moments of some sites drop down to zero, the multi-**Q** state is distorted. But the corresponding quantum disordered state can not be described within the framework of a LSW approach. So it is possible that other type of strong quantum fluctuations drive the system to a QSL via distabilizing the multi-**Q** phase. In other words, the phase diagram of the system under strong quantum fluctuations remains to be explored, and it would be interesting to know the form of the elementary excitations of the corresponding phase there.

For the $YbMgGaO_4$ compound, the seemingly divergent magnetic susceptibility and the power-law behavior of the specific heat $C_V \sim T^{2/3}$ suggest absence of long-range magnetic order. Assuming that the system can be described by the model Hamiltonian in Eq. (1), the superexchange couplings of the system have been recently estimated from ESR measurements. It is found that $|J_{\pm\pm}/J_{zz}| \sim 0.16$ and $|J_{z\pm}/J_{zz}| \sim 0.04$.[12] These parameters suggest that the system is very close to the boundary between the Néel and the multi-**Q** phase regime, as shown in Fig. 1(a). But according to our LSW calculation, the ground state is still magnetically ordered even for $S = 1/2$. To reconcile the theory with the experimental findings, on the one hand, other experimental measurements, such as neutron and/or Raman scattering should be done to confirm or give better estimates of the exchange couplings. It would be especially important to accurately determine the value of the $J_{z\pm}$ coupling, because our results show that a spin liquid state would be much easier to be stabilized with a large $J_{z\pm}$ value. On the other hand, other perturbations beyond the present model but likely existed in the real materials, such as the longer ranged exchange couplings, the ring exchange interaction, or disorder, may further disturb the long-range magnetic order and drive the system toward a spin liquid[2–6].

In our model, the multi-**Q** states lie in large areas in the parameter space of the phase diagram. One may be curious whether similar states exist in other spin-orbit coupled system. Indeed, similar incommensurate ordered states have been found in a number of theoretical models, such as the Heisenberg-Kitaev model on triangular lattice, and Heisenberg models on hyperhoneycomb and hyperkagome lattices.[22–26] There are also some experimental evidences of these exotic magnetic states[27,28]. However, to our knowledge, the microscopic origin and physical properties of these states are not yet well addressed. Given the similar magnetic structures of these incommensurate states to the multi-**Q**, they likely share the same origin: as the symmetry is lowered by the SOC induced anisotropic interactions, the spin wave of the original commensurate magnetic ground state (denoted as the parent state) is distabilized, and the magnons condense at a nearby incommensurate wave vector. For example, in the Kitaev-Heisenberg model on the triangular lattice,

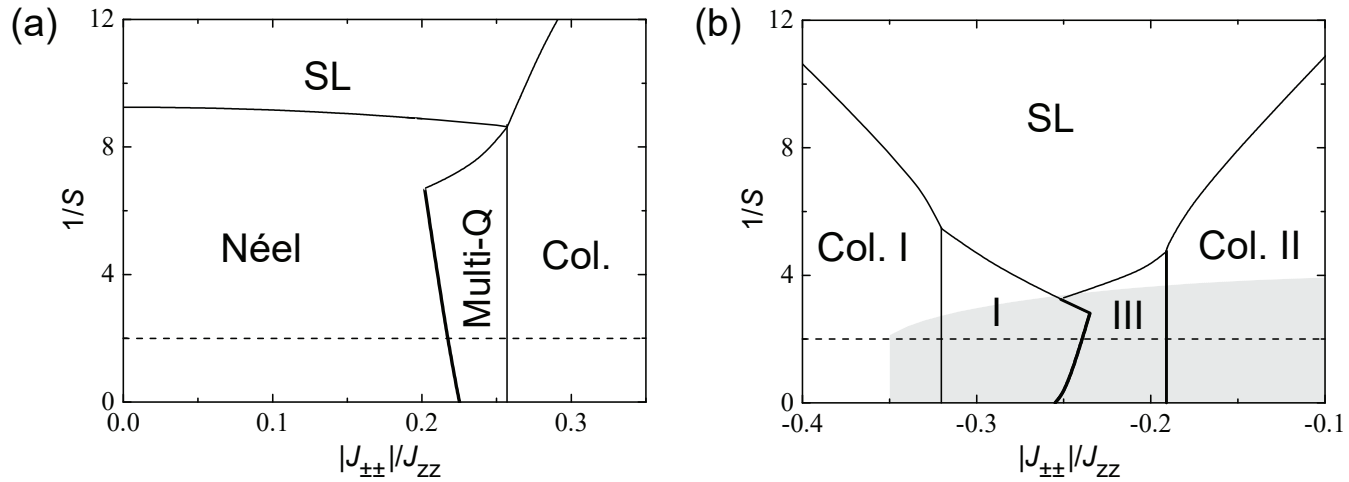

FIG. 6. Phase diagrams taking into account the quantum correction from linear spin-wave theory for (a): $J_{z\pm} = 0$ and (b): $J_{z\pm} = 0.9$. Thinner solid curves correspond to second-order transitions and thicker solid curves correspond to first-order transitions. The dashed line marks $S = 1/2$. In panel (b), the gray shading shows the regime where the Néel state is a metastable state (which has an energy higher than other ordered states).

once a finite Kitaev exchange coupling is added to the antiferromagnetic Heisenberg interaction, the Néel AFM ground state immediately becomes unstable to an incommensurate Z_2 vortex crystal.[22,23] This is clearly seen in the spin-wave spectrum of the Néel AFM state, which is destabilized around M point of the Brilluion zone as soon as the system goes away from the Heisenberg point. Interestingly, the nature of the incommensurate state is closely connected to the properties of its parent state. Still in the Heisenberg-Kitaev model, the parent state of the Z_2 vortex crystal state is the three-sublattice 120° Néel AFM state, in which the order parameter space is SO(3), and Z_2 point topological defects are allowed.[29] Therefore, the topologically nontrivial Z_2 vortice crystal is stabilized when its parent state is disturbed.[22,23] However, for the model Hamiltonian in Eq. (1), the parent state of the multi-$\mathbf{Q}$ states are the two-sublattice collinear states. Therefore, the multi-$\mathbf{Q}$ states are topologically trivial. It would be interesting to further explore whether such a scenario generally holds for the magnetism in systems with strong spin-orbit coupling.

VI. CONCLUSIONS

In summary, we investigate the semiclassical phase diagram of an effective spin model describing the strongly spin-orbit coupled local moments in $YbMgGaO_4$. We identify three novel incommensurate multi-$\mathbf{Q}$ antiferromagnetic states in the classical phase diagram of this model. We study the spin excitations of these states using a linear spin-wave theory, and find that the spin excitation spectra contain multiple branches, and the excitation gap can be vanishingly small. With the linear spin-wave theory, we further study the effects of quantum fluctuations on the classical magnetic orders, and find that all these phases are stable under weak to moderate quantum fluctuations. A spin liquid phase is stabilized for sufficiently strong quantum fluctuations when the anisotropic exchange coupling $|J_{z\pm}|$ is large.

VII. ACKNOWLEDGEMENT

We would like to acknowledge useful discussions with G. Chen, P. Holdsworth, Y.-D. Li, Y. S. Li, Z.-X. Liu, B. Normand, T. Roscilde, Q. M. Zhang, Q. Luo and J. Zhao. This work was supported in part by the National Program on Key Research Project Grant number 2016YFA0300500 (X.Q.W. and R.Y.), by the National Science Foundation of China Grant number 11574200 (X.Q.W.), by the National Science Foundation of China Grant number 11374361 and the Fundamental Research Funds for the Central Universities and the Research Funds of Remnin University of China Grant number 14XNLF08 (R.Y.). R.Y. acknowledge the hospitality of the Physics Laboratory at ENS de Lyon.

Appendix A: Construction of multi-Q states within a modified Luttinger-Tisza approach

States produced by the original LT method have single-$\mathbf{Q}$ structure, which means only $\mathbf{S}_{\pm\mathbf{Q}}$ is nonzero among all Fourier components. One can easily check that, if the ordering wave vector $\mathbf{Q}$ is time reversal invariant(TRI , which means $\mathbf{Q} = -\mathbf{Q} + \mathbf{G}$) momentum, such state always satisfy all local constraints (6) and produces physical *collinear* groundstates; if $\mathbf{Q}$ is non-TRI, by taking $\mathbf{q} = 2\mathbf{Q}$ in (6), we have $\mathbf{S}_{\mathbf{Q}} \cdot \mathbf{S}_{\mathbf{Q}} = 0$, which implies that at least two component in $\mathbf{S}_{\mathbf{Q}}$ must be nonzero. Therefore, if the minimum of the eigenvalue of the tensor $\mathsf{J}_{\mathbf{Q}}$ happens to be at least two-fold degenerate, LT method can still produce physical *helical* groundstates, otherwise such method cannot produce physical groundstates satisfying (6).

In general, if a system has continuous $U(1)$ symmetry, in some parameter regime the minimum of the eigenvalue of $\mathsf{J}_{\mathbf{Q}}$ have degeneracy, so LT method still works. However, the model we study has only discrete symmetries, LT method immediately fails once the minimum of the eigenvalue of $\mathsf{J}_{\mathbf{Q}}$ deviates $\mathbf{Q}_0$. Nevertheless, such multi-$\mathbf{Q}$ groundstates can still be well reconstructed in a modified version of LT method by introducing finite Fourier components $\mathbf{S}_{\mathbf{Q}}$ on multiple $\mathbf{Q}$'s based on the collinear states so as to minimize the energy on the premise of satisfying all local constraints (8).

For pure collinear state there is only one nonzero component $\mathbf{S}_{\mathbf{Q_0}}$ where $\mathbf{Q}_0$ is the collinear ordering wave vector. If there exists some (non-TRI) $\mathbf{Q}_1$ point where the eigenstate of $\mathsf{J}_{\mathbf{Q_1}}$ is lower than the minimum eigenvalue of $\mathsf{J}_{\mathbf{Q_0}}$, the system may tend to partially condense at $\pm\mathbf{Q}_1$ points in order to gain more energy. By taking $\mathbf{q} = 2\mathbf{Q_1}$ in (6) we find that we further need to introduce $\mathbf{Q}_2 = [2\mathbf{Q}_1 - \mathbf{Q}_0]$ component in order to satisfy local constraint, i.e. $\mathbf{S}_{\mathbf{Q}_1} \cdot \mathbf{S}_{\mathbf{Q}_1} + \mathbf{S}_{\mathbf{Q}_0} \cdot \mathbf{S}_{\mathbf{Q}_2} + \mathbf{S}_{\mathbf{Q}_2} \cdot \mathbf{S}_{\mathbf{Q}_0} = 0$.

From the above equation we can see that the magnitude of $\mathbf{S}_{\mathbf{Q}_2}$ is about order of $|\mathbf{S}_{\mathbf{Q}_1}|^2/|\mathbf{S}_{\mathbf{Q}_0}|$. In general, the eigenvalues of $\mathsf{J}_{\mathbf{Q_2}}$ are much larger than the minimum ones of $\mathsf{J}_{\mathbf{Q_0}}$ and $\mathsf{J}_{\mathbf{Q_1}}$, so $|\mathbf{S}_{\mathbf{Q}_2}|$ is in principle very small in order not to cause too much energy penalty. Following the same procedure, by taking $\mathbf{q} = 2\mathbf{Q_2}$ in (6) we find that other finite Fourier components, say $\mathbf{S}_{\pm\mathbf{Q}_3}$, in order to satisfy such constraint. In principle, following this way of construction, an infinite series of finite $\mathbf{S}_{\mathbf{Q}_n}$ must be introduced in order to satisfy (6) rigorously. However, their magnitude decays exponentially and for $n > 2$, these components are generally too small to be detected (no greater than the order of $|\mathbf{S}_{\mathbf{Q}_1}|^3/|\mathbf{S}_{\mathbf{Q}_0}|^2$) and have no physical significance, so we truncate the series at $n = 2$. Although the truncated configuration $\{\mathbf{S}_{\mathbf{Q}_0}, \mathbf{S}_{\pm\mathbf{Q}_1}, \mathbf{S}_{\pm\mathbf{Q}_2}\}$ do not exactly satisfy (6), such an approximation turns out to be very well reconstructing multi-$\mathbf{Q}$ configurations.

The groundstate is therefore obtained by minimizing

$$E\{\mathbf{S}_{\mathbf{Q}_0},\mathbf{S}_{\mathbf{Q}_1},\mathbf{S}_{\mathbf{Q}_2}\}=\mathbf{S}^*_{\mathbf{Q}_0}\cdot \mathsf{J}_{\mathbf{Q}_0}\cdot\mathbf{S}_{\mathbf{Q}_0} + 2\mathbf{S}^*_{\mathbf{Q}_1}\cdot \mathsf{J}_{\mathbf{Q}_1}\cdot\mathbf{S}_{\mathbf{Q}_1}+2\mathbf{S}^*_{\mathbf{Q}_2}\cdot \mathsf{J}_{\mathbf{Q}_2}\cdot\mathbf{S}_{\mathbf{Q}_2} \tag{A1}$$

within constraints (by taking $\mathbf{q}=\mathbf{G}$, $\mathbf{Q}_0+\mathbf{Q}_1$, $2\mathbf{Q}_1$, $\mathbf{Q}_1+\mathbf{Q}_2$ in (6) respectively)

$$|\mathbf{S}_{\mathbf{Q}_0}|^2+|\mathbf{S}_{\mathbf{Q}_1}|^2+|\mathbf{S}_{\mathbf{Q}_2}|^2=NS^2 \tag{A2}$$
$$\mathbf{S}_{\mathbf{Q}_0}\cdot\mathbf{S}_{\mathbf{Q}_1}+\mathbf{S}_{\mathbf{Q}_1}\cdot\mathbf{S}_{-\mathbf{Q}_2}=0 \tag{A3}$$
$$\mathbf{S}_{\mathbf{Q}_1}\cdot\mathbf{S}_{\mathbf{Q}_1}+2\mathbf{S}_{\mathbf{Q}_0}\cdot\mathbf{S}_{\mathbf{Q}_2}=0 \tag{A4}$$
$$\mathbf{S}_{\mathbf{Q}_1}\cdot\mathbf{S}_{\mathbf{Q}_2}=0 \tag{A5}$$

We can see from (A3) and (A5) that $\mathbf{S}_{\mathbf{Q}_1}\perp\mathbf{S}_{\mathbf{Q}_2}$ and approximately $\mathbf{S}_{\mathbf{Q}_1}\perp\mathbf{S}_{\mathbf{Q}_0}$ (as the magnitude of $\mathbf{S}_{-\mathbf{Q}_2}$ is generally much smaller than $\mathbf{S}_{\mathbf{Q}_0}$). By taking the energy optimization, we find that the energy minimum of multi-**Q** I/II phases satisfy $\mathbf{S}_{\mathbf{Q}_2}\parallel\mathbf{S}_{\mathbf{Q}_0}$, i.e. all $\mathbf{S}_{\mathbf{Q}}$'s are in the same plane. So multi-**Q** I/II states are coplanar, with all spins lying in the plane spanned by $\mathbf{S}_{\mathbf{Q}_0}$ and $\mathbf{S}_{\mathbf{Q}_1}$. However, such relation do not satisfy for multi-**Q** III phases, which implies that multi-**Q** III states are not coplanar.

Also, we find that the phase of $\mathbf{S}_{\mathbf{Q}_1}$, which is relavent to the spin configuration, do not effect the energy within our approximation.

Appendix B: Linear spin wave method

Here we present our linear spin wave method which applies to systems with periodic structure in classical configuration. Suppose the configuration can be devided into M sublattices. This method apparently works for Néel(3 sublattices) and collinear(2 sublattices) order. For multi-**Q** states one can still apply such method if we carefully choose the model parameters and the cluster size such that all ordering wavevectors well matches the reciprocal lattice of the cluster.

The method is performed as following[15–17]. Suppose that ground state has classical configuration $\{\mathbf{n}_{ns}\}$ where $\mathbf{n}_{ns}$ is the unit vector pointing direction of the spin at the site i labeled by magnetic unit cell index n and sublattice index s. Since the spin direction only depends on the sublattice index s, i.e. $\mathbf{n}_{ns}=\mathbf{n}_s$. For each $\mathbf{n}_s$ one can always find a rotation operation $R_s\in SO(3)$ that rotates $\hat{z}$ to $\mathbf{n}_s$ direction, i.e., $\mathbf{n}_s=R_s\hat{z}$.

Introduce $\mathbf{S}_{ns}=R_s\tilde{\mathbf{S}}_{ns}$, so each $\tilde{\mathbf{S}}_{ns}$ has classical configuration ferromagnetically aligned along $\hat{z}$ direction. Then we perform H-P transformation for $\tilde{\mathbf{S}}_{ns}$.

$$\begin{aligned}\tilde{S}^z_{ns}&=S-b^\dagger_{ns}b_{ns}\\ \tilde{S}^+_{ns}&=\sqrt{2S-b^\dagger_{ns}b_{ns}}\,b_{ns}\\ \tilde{S}^-_{ns}&=b^\dagger_{ns}\sqrt{2S-b^\dagger_{ns}b_{ns}}\end{aligned} \tag{B1}$$

At the LSW level, $\mathbf{S}_{ns}$ can be expressed as

$$\mathbf{S}_{ns}=\sqrt{\frac{S}{2}}(\mathbf{u}^*_s b_{ns}+\mathbf{u}_s b^\dagger_{ns})+\mathbf{v}_s(S-b^\dagger_{ns}b_{ns}) \tag{B2}$$

where $u^\mu_s=R^{\mu x}_s+iR^{\mu y}_s$, and $v^\mu_s=R^{\mu z}_s$ for $\mu=x,y,z$ components.

Take eq. (B2) into the Hamiltonian (1), after Fourier transformation

$$b_{ns}=\sqrt{\frac{M}{N}}\sum_{\mathbf{k}\in MBZ}b_{\mathbf{k}s}e^{i\mathbf{R}_{ns}\cdot\mathbf{k}} \tag{B3}$$

The Hamiltonian can be rewritten in terms of boson bilinears at the LSW level

$$H=E_0+\frac{1}{2}\sum_{\mathbf{k}\in MBZ}[\Psi(\mathbf{k})^\dagger h(\mathbf{k})\Psi(\mathbf{k})-\frac{1}{2}\mathrm{tr}\,h(\mathbf{k})] \tag{B4}$$

where E_0 is the classical energy, $\Phi(\mathbf{k})=\left[b_{\mathbf{k}1},\cdots,b_{\mathbf{k}M},b^\dagger_{-\mathbf{k}1},\cdots,b^\dagger_{-\mathbf{k}M}\right]^T$, $h(\mathbf{k})$ is a $2M\times 2M$ Hermitian matrix.

H can be diagonalized via Bogoliubov transformation$\Psi(\mathbf{k})=T_{\mathbf{k}}\Phi(\mathbf{k})$ where $\Phi(\mathbf{k})=\left[\beta_{\mathbf{k}1},\cdots,\beta_{\mathbf{k}M},\beta^\dagger_{-\mathbf{k}1},\cdots,\beta^\dagger_{-\mathbf{k}M}\right]^T$ and $T_{\mathbf{k}}\in SU(M,M)$ in order to ensure bosonic commutation rules of Bogoliubov quasiparticles β's.

The dianonalized Hamiltonian reads

$$\begin{aligned}H&=E_0+\frac{1}{2}\sum_{\mathbf{k}\in MBZ}[\Phi(\mathbf{k})^\dagger E(\mathbf{k})\Phi(\mathbf{k})-\frac{1}{2}\mathrm{tr}\,h(\mathbf{k})]\\ &=E_0+E_r+\sum_{\mathbf{k}\in MBZ}\omega_{\mathbf{k}s}\beta^\dagger_{\mathbf{k}s}\beta_{\mathbf{k}s}\end{aligned} \tag{B5}$$

where $E(\mathbf{k})=\mathrm{diag}[\omega_{\mathbf{k}1},\cdots,\omega_{\mathbf{k}M},-\omega_{-\mathbf{k}1},\cdots,-\omega_{-\mathbf{k}M}]$ and $E_r=\frac{1}{4N}\sum_{\mathbf{k}\in MBZ}\mathrm{tr}\,[E(\mathbf{k})-h(\mathbf{k})]$ is the zero point energy correction due to quantum fluctuation.

Following[15], at zero temperature, the ordered moment reduction for the s'th sublattice Δm_s reads

$$\begin{aligned}\Delta m_s&=\frac{M}{N}\langle\sum_n b^\dagger_{ns}b_{ns}\rangle\\ &=\frac{M}{N}\sum_{\mathbf{k}\in MBZ}(T_{\mathbf{k}}T^\dagger_{\mathbf{k}})_{s+M,s+M}\end{aligned} \tag{B6}$$

and the dynamical structrual factor take the form

$$S^{\mu\nu}(\mathbf{k},\omega)=\frac{S}{2N}\sum_{s=1}^{M}[T^\dagger_{\mathbf{k}}\mathbf{U}^\mu(\mathbf{U}^\nu)^\dagger T_{\mathbf{k}}]_{s+M,s+M}\delta(\omega-\omega_{\mathbf{k}s})$$

where $\mathbf{U}^\mu=[u^\mu_1,\cdots,u^\mu_M,(u^\mu_1)^*,\cdots,(u^\mu_M)^*]^T$ are vectors in $2M$ dimension.

[1] L. Balents, Nature **464**, 199 (2010).
[2] G. Misguich, C. Lhuillier, B. Bernu, and C. Waldtmann, Phys. Rev. B **60**, 1064 (1999).
[3] O. I. Motrunich, Phys Rev. B **72**, 045105 (2005).
[4] R. Kaneko, S. Morita, and M. Imada, J. Phys. Soc. Jpn. **83**, 093707 (2014).
[5] P. H. Li, R. F. Bishop, and C. E. Campbell, Phys. Rev. B **91**, 014426 (2015).
[6] K. Watanabe, H. Kawamura, H. Nakano, and T. Sakai, J. Phys. Soc. Jpn. **83**, 034714 (2014).
[7] A. Kitaev, Annals of Physics **321**, 2 (2006), january Special Issue.
[8] Z. Nussinov and J. van den Brink, Rev. Mod. Phys. **87**, 1 (2015).
[9] K. KI and D. Khomskii, Sov. Phys. Usp **25**, 231 (1982).
[10] L. Messio, O. Cpas, and C. Lhuillier, Phys. Rev. B **81**, 064428 (2010).
[11] Y. Li, H. Liao, Z. Zhang, S. Li, F. Jin, L. Ling, L. Zhang, Y. Zou, L. Pi, and Z. Yang, Sci. Rep. **5** (2015).
[12] Y. Li, G. Chen, W. Tong, L. Pi, J. Liu, Z. Yang, X. Wang, and Q. Zhang, Phys. Rev. Lett. **115**, 167203 (2015).
[13] J. Luttinger and L. Tisza, Phys. Rev. **70**, 954 (1946).
[14] Y.-D. Li and G. Chen, arXiv:1512.02151 (2015).
[15] S. Toth and B. Lake, J. Phys.: Cond. Mat. **27**, 166002 (2015).
[16] S. Petit, Collection SFN **12**, 105 (2011).
[17] D. C. Wallace, Phys. Rev. **128**, 1614 (1962).
[18] R. R. Singh and D. A. Huse, Phys. Rev. Lett. **68**, 1766 (1992).
[19] L. Capriotti, A. E. Trumper, and S. Sorella, Phys. Rev. Lett. **82**, 3899 (1999).
[20] C. Wu, Phys. Rev. Lett. **100**, 200406 (2008).
[21] O. Zaharko, P. Fischer, A. Schenck, S. Kunii, P.-J. Brown, F. Tasset, and T. Hansen, Phys. Rev. B **68**, 214401 (2003).
[22] I. Rousochatzakis, U. K. Rssler, J. van den Brink, and M. Daghofer, Phys. Rev. B **93**, 104417 (2016).
[23] M. Becker, M. Hermanns, B. Bauer, M. Garst, and S. Trebst, Physical Review B **91**, 155135 (2015).
[24] E. K.-H. Lee, J. G. Rau, and Y. B. Kim, arXiv:1506.06746 (2015).
[25] E. K.-H. Lee and Y. B. Kim, Phys. Rev. B **91**, 064407 (2015).
[26] T. Mizoguchi, K. Hwang, E. K.-H. Lee, and Y. B. Kim, arXiv:1603.00469 (2016).
[27] A. Biffin, R. Johnson, I. Kimchi, R. Morris, A. Bombardi, J. Analytis, A. Vishwanath, and R. Coldea, Phys. Rev. Lett. **113**, 197201 (2014).
[28] A. Biffin, R. Johnson, S. Choi, F. Freund, S. Manni, A. Bombardi, P. Manuel, P. Gegenwart, and R. Coldea, Phys. Rev. B **90**, 205116 (2014).
[29] H. Hawamura and S. Miyashita, J. Phys. Soc. Jpn. **53**, 4138 (1984).